Electronic Supporting Information

Ethylene glycol-mediated one-pot synthesis of Fe incorporated α-$Ni(OH)_2$ nanosheets with enhanced intrinsic electrocatalytic activity and long-term stability for alkaline water oxidation

*Gouri Tudu, Sourav Ghosh‡, Sagar Ganguli‡, Heramba V. S. R. M. Koppisetti, Harish Reddy Inta and Venkataramanan Mahalingam**

Department of Chemical Sciences, Indian Institute of Science Education and Research (IISER) Kolkata, Mohanpur, West Bengal, 741246, India.

* E-mail: mvenkataramanan@yahoo.com; Fax: 91-33-25873020; Tel: +91(0)9007603474.

‡ Equal contribution

1. EXPERIMENTAL SECTION

1.1. Materials. Iron nitrate nonahydrate [$Fe(NO_3)_3.9H_2O$], Nickel acetate tetrahydrate [$Ni(OCOCH_3)_2.4H_2O$], N,N,N′,N′-Tetramethylethane-1,2-diamine (TMEDA), Hexamethylenetetramine (HMTA) were purchased from Sigma Aldrich. Ethylene glycol, Urea, potassium hydroxide (KOH) were purchased from Merck. All chemicals were used without any further purification.

1.2. Catalyst Synthesis.

Preparation of nickel iron hydroxide in water-ethylene glycol mixture, [$NiFe(OH)_2$]:

In a 250 mL borosilicate glass bottle (Fisher brand), 1.6 mmol of $Ni(OCOCH_3)_2 \cdot 4H_2O$ (0.398 g) and 0.4 mmol of $Fe(NO_3)_3 \cdot 9H_2O$ (0.162 g) [for $Ni_xFe_{(1-x)}(OH)_2$ (where, x= 0.8) preparation] were dissolved in 24 mL of distilled water. Subsequently 12 mL of ethylene glycol (EG) was added to it and stirred for 10 minutes. Next, 12 mmol of N,N,N′,N′-Tetramethylethane-1,2-diamine (TMEDA) (1.8 mL) was added to the reaction mixture and heated at 80 ℃ for 12 hours on continuous stirring. The reaction mixture was then centrifuged and washed several times with distilled water and methanol. The obtained pear green color solid was dried in oven at 65 ℃. In addition, for optimization of the catalyst material the ratio of Ni and Fe was also varied in $Ni_xFe_{(1-x)}(OH)_2$ (x= 0.9 and 0.7) keeping the reaction conditions same.

To investigate the role of each reactant, the same procedure and conditions were followed for control synthesis of the materials by excluding one of each component at a time present in the above system. Thus, $Ni(OH)_2$ was synthesized by avoiding the use of iron in the synthesis whereas $Fe(OH)_3$ was obtained in the absence of nickel source. To understand the role and effect of the solvents in the synthesis, $NiFe(OH)_2$ materials [i.e. $Ni_{0.8}Fe_{0.2}(OH)_2$] were prepared in only water, only EG and by varying the ratio of EG and water (EG: water= 1:20, 1:10, 1:5, 1:2, 1:1, 2:1 and 5:1) under the identical reaction conditions as mentioned above. In absence of ethylene glycol, i.e. in pure aqueous medium the obtained $NiFe(OH)_2$ material was assigned as $NiFe(OH)_2$-Aq. When the reaction was performed in pure ethylene glycol the obtained nickel iron hydroxide material was assigned as $NiFe(OH)_2$-EG. Further to investigate the effect of both iron and EG, the control experiment was done by synthesizing $Ni(OH)_2$ in absence of both iron source and EG. To check the importance of TMEDA, synthesis of $NiFe(OH)_2$ was performed

without using TMEDA and no precipitation or product was formed. In addition to TMEDA, $NiFe(OH)_2$ was also prepared using other conventional bases like Hexamethylenetetramine (HMTA) and urea for electrocatalytic comparison study following the same reaction conditions.

The sample IDs of the main as-prepared samples have been summarized in the **Table S1**.

1.3. Characterization Techniques. The PXRD patterns were recorded using a Rigaku MiniFlex600 diffractometer attached with a D/teX Ultra detector and Cu Kα source operating at 15 mA and 40 kV. The scan range was set from 5 to 80° 2θ with a step size of 0.02° and a count time of 2 s. FT-IR measurements were performed in a Perkin Elmer Spectrum instrument. Field emission SEM images and EDAX were acquired on a SUPRA 55-VP instrument with patented GEMINI column technology. Prior to loading the samples into the chamber, they were coated with a thin layer of gold-palladium in order to avoid charging effects. TEM images were acquired on a JEM 2100F field emission transmission electron microscope operating at 200 kV. Nitrogen adsorption-desorption measurements were conducted at 77 K with a Micromeritics Gemini VII-2390t instrument. The samples were outgassed in vacuum at 180 °C for 2 h prior to measurements. The inductively coupled plasma atomic emission spectroscopy (ICP-AES) analysis was performed in ACROS, Simultaneous ICP Spectrometer manufactured by SPECTRO Analytical Instruments GmbH, Germany. The surface chemistry of the samples was analyzed using X-ray photoelectron spectroscopy (XPS, PHI 5000 VersaProbe II, ULVAC-PHI Inc.,USA) equipped with micro-focused (200 μm, 15 KV) monochromatic Al-Kα X-Ray source ($h\nu$ =1486.6 eV).

1.4. Electrochemical Measurements.

1.4.1. Electrode ink preparation.

1.4.1.1. Glassy carbon (GC) as substrate: 4 mg of sample was dispersed in 500 µL distilled water, 500 µL of ethanol and 50 µL Polyvinylidene fluoride (PVDF) binder solution [8 mg PVDF in 1 mL N-Methyl-2-pyrrolidone (NMP)] and sonicated for 20 minutes. 4 µL of the catalyst ink was drop-casted on the GC electrode (surface area = 0.0707 cm^2) and dried in oven at 55 ℃. Therefore, the total catalyst amount loaded on GC was 0.0152 mg, and the catalyst loading is 0.215 mg/cm^2 for GC substrate for all the samples.

1.4.1.2. Carbon paper as substrate: Each sample was mixed well with PVDF (w/w= 9:1) using ethanol in a mortar and pestle to prepare sample-PVDF stock. Then 2.2 mg of sample-PVDF stock was dispersed in 240 µL of ethanol and sonicated for 20 minutes. Next, 10 µL of the catalyst ink was drop-casted on each side of the carbon paper (surface area = 0.25 cm^2) and dried in oven at 55 ℃. Therefore, the total catalyst amount loaded on carbon paper was 0.165 mg, and the catalyst loading is 0.66 mg/cm^2 on carbon paper for all the samples. The experiments like stability study, Faradaic efficiency study have been performed on carbon paper substrate only.

1.4.2. Electrochemical Measurements. All electrochemical measurements were performed on a computer-controlled electrochemical workstation (BioLogic SP-300), using three-electrode cell comprising the materials on glassy carbon (GC) electrode, Pt wire, and Ag/AgCl (3.5 M KCl) as the working, counter, and reference electrode, respectively. For OER measurements, 1 (M) KOH solution was used and the potential scale was calibrated to the reversible hydrogen electrode (RHE). The catalysts were first preconditioned by performing CV within the potential range 1-1.8 (0-0.6 V vs Ag/AgCl) V, for 20 cycles at scan rate 50 mV s^{-1} followed by 2 cycles at scan

rate 5 mV s^{-1} in order to evaluate the OER. Electrochemical performance was further scrutinized by iR-corrected backward LSV scan from R_u (uncompensated resistance). Mechanism of alkaline OER was further anticipated through variation of pH of electrolyte. In addition, electrochemical impedance spectroscopy (EIS) was examined with the same set up in the frequency range 100 kHz to 10 Hz at voltage 0.5 V. The performance of electrocatalysts were further analyzed by double layer capacitance (C_{dl}) which is known as a non-destructive parameter for estimation of electrochemical surface area (ECSA). The measurement of C_{dl} was performed in organic electrolyte solution (acetonitrile containing 0.15 M KPF_6) as suggested by Surendranath *et al*. To study the stability of the best sample, chronopotentiometry technique was carried out for 7 days for carbon-paper supported electrocatalyst. CV measurement was also recorded both before and after the chronopotentiometry to compare the change in activity after prolong stability. Finally, Faradaic efficiency of the catalyst was checked by chronocoulometry technique in 1(M) KOH.

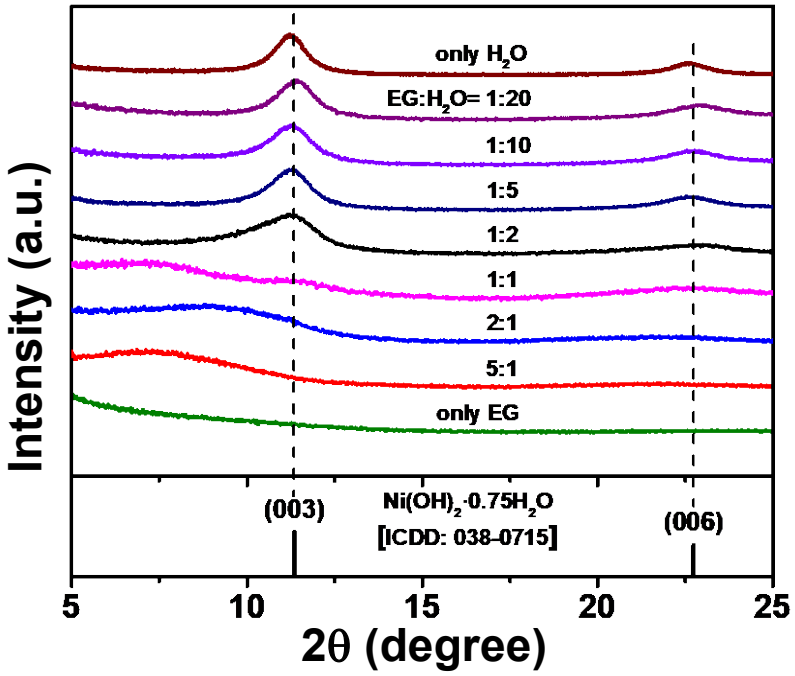

Figure S1. PXRD patterns of $NiFe(OH)_2$ samples by varying the ratio of EG to water during synthesis (2θ range from 5 to 25 degree).

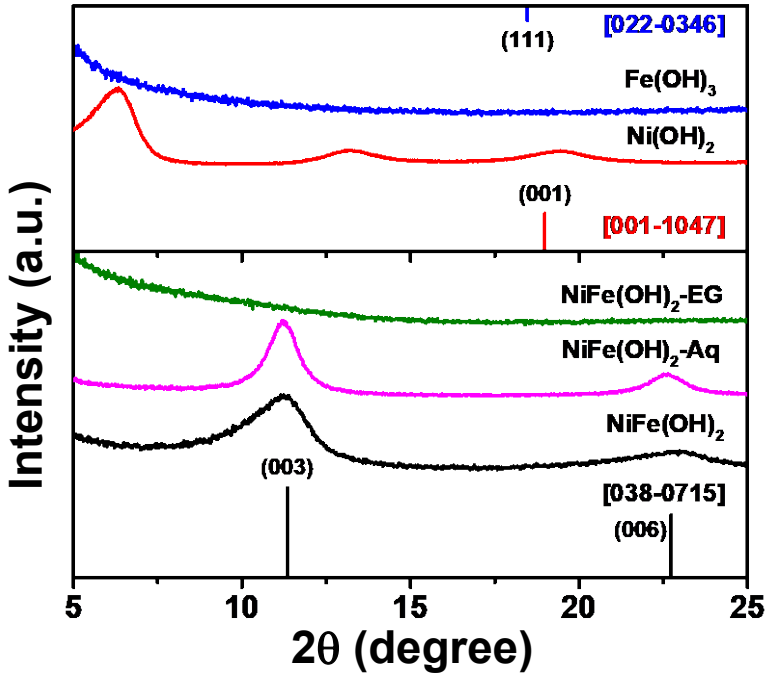

Figure S2. PXRD patterns of as-prepared $Ni(OH)_2$, $NiFe(OH)_2$-Aq, $NiFe(OH)_2$-EG, $NiFe(OH)_2$ and $Fe(OH)_3$ powder samples (2θ range from 5 to 25 degree).

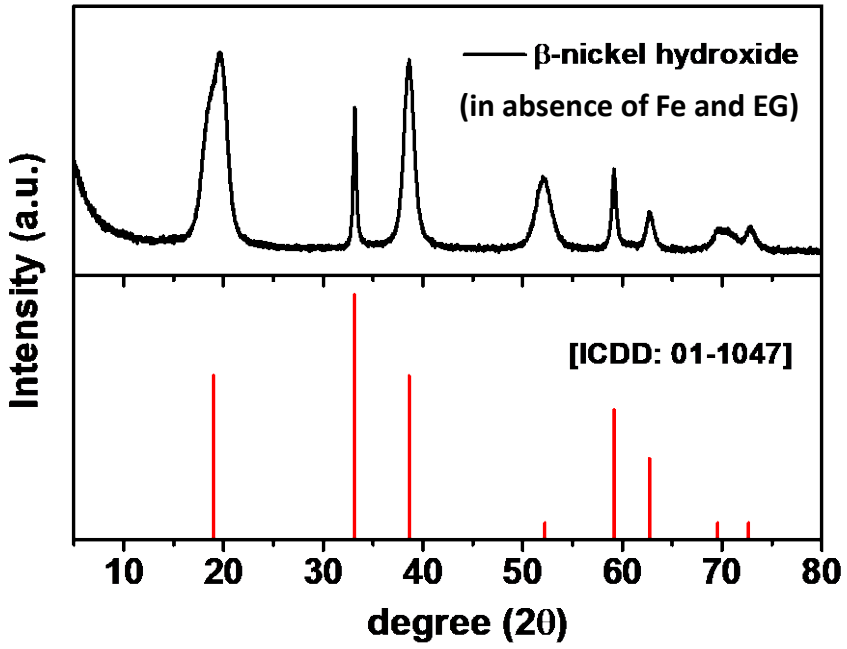

Figure S3. PXRD pattern of $Ni(OH)_2$ obtained after synthesizing $Ni(OH)_2$ without using any Fe-source and EG, showing formation of pure phase β-$Ni(OH)_2$.

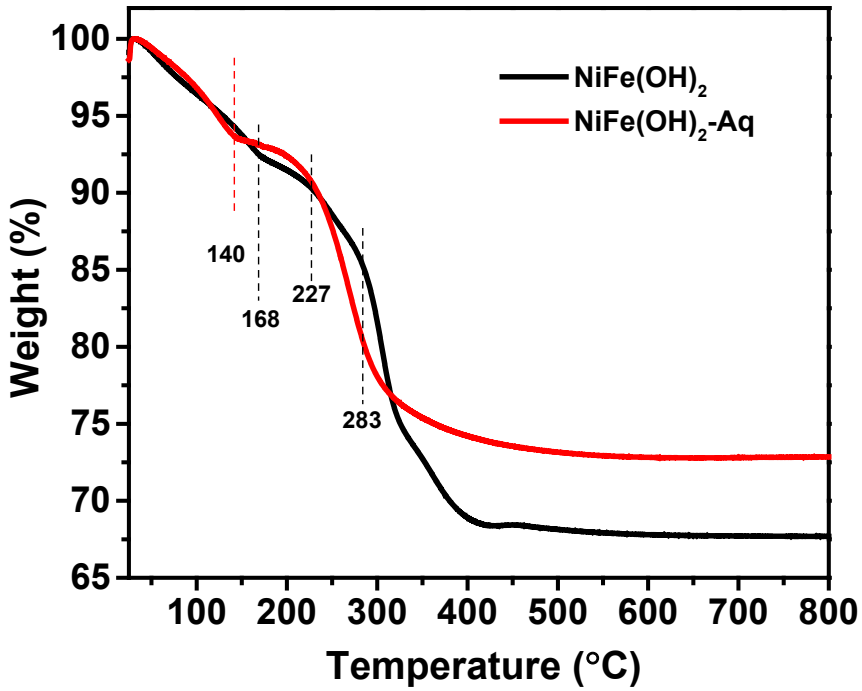

Figure S4. TGA plots of $NiFe(OH)_2$-Aq and $NiFe(OH)_2$, the analysis done at a heating rate of 10 °C/ min.

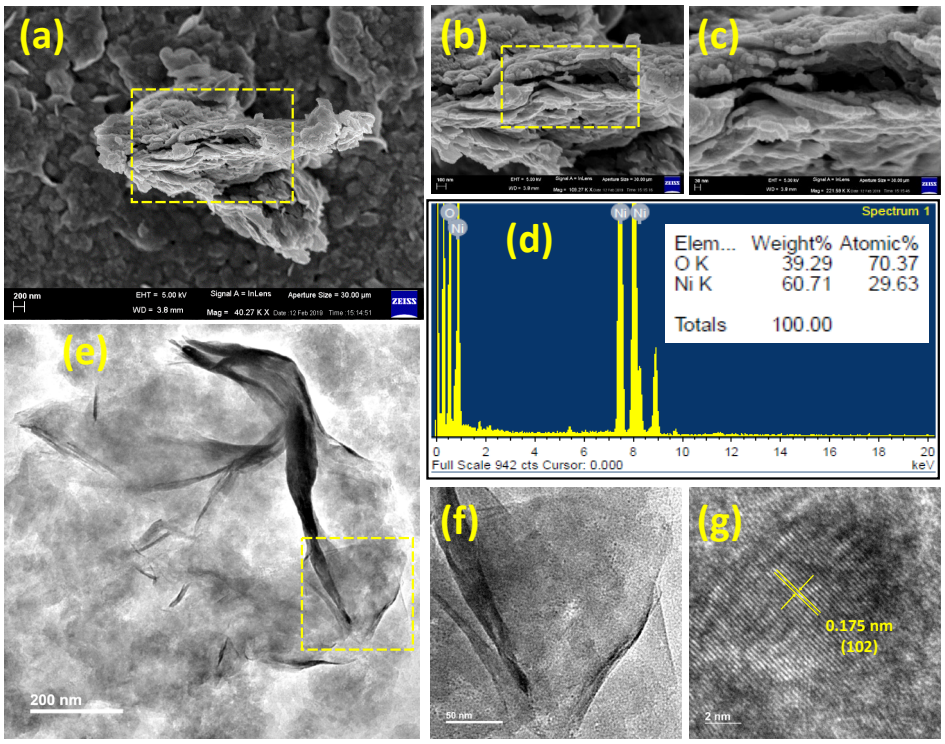

Figure S5. (a-c) FESEM images, (d) EDS data, (e, f) TEM images and (g) HRTEM image of $Ni(OH)_2$ electrocatalyst.

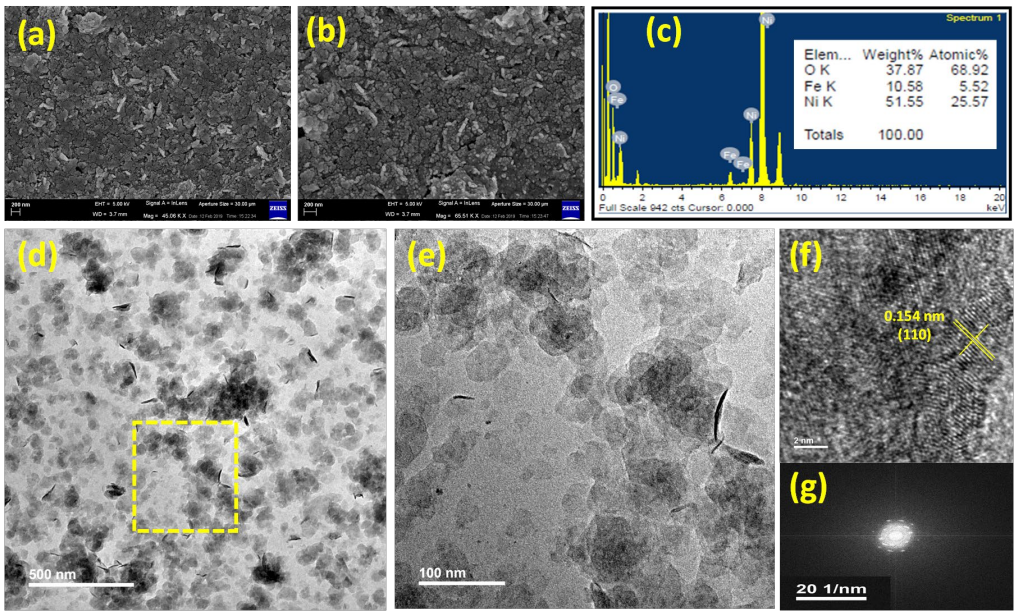

Figure S6. (a, b) FESEM images, (c) EDS data, (d, e) TEM images, (f) HRTEM image and (g) corresponding FFT of the HRTEM image of $NiFe(OH)_2$-Aq electrocatalyst.

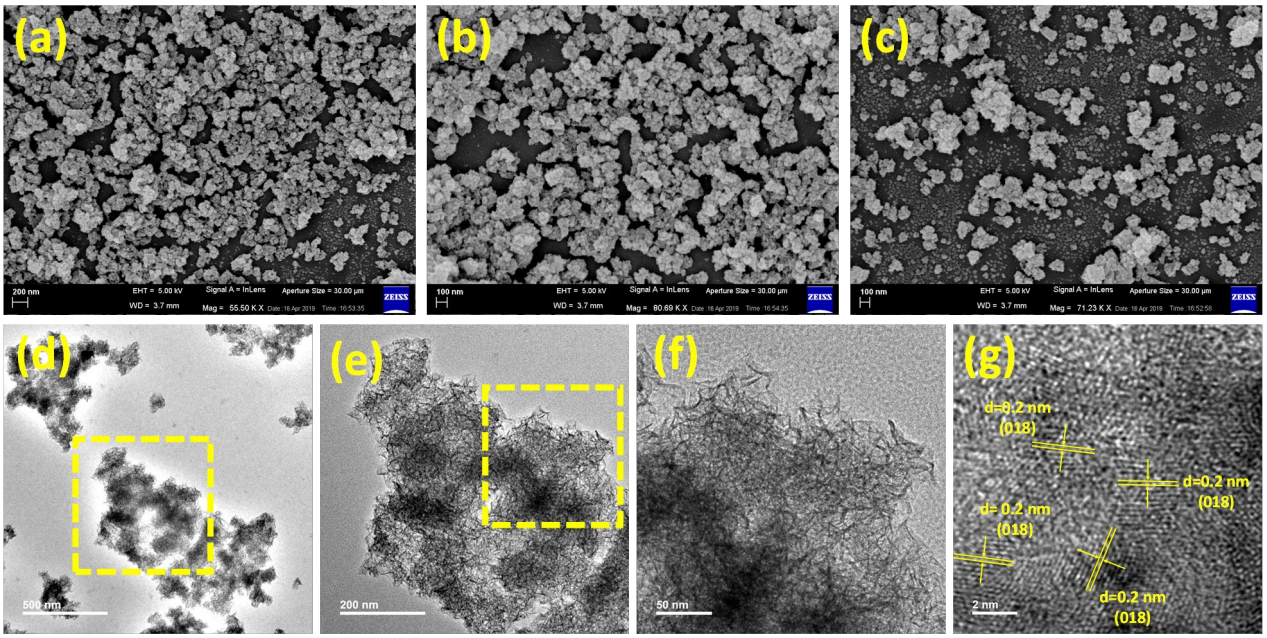

Figure S7. (a-c) FESEM images, (d-f) TEM images and (g) HRTEM image of $NiFe(OH)_2$-EG electrocatalyst.

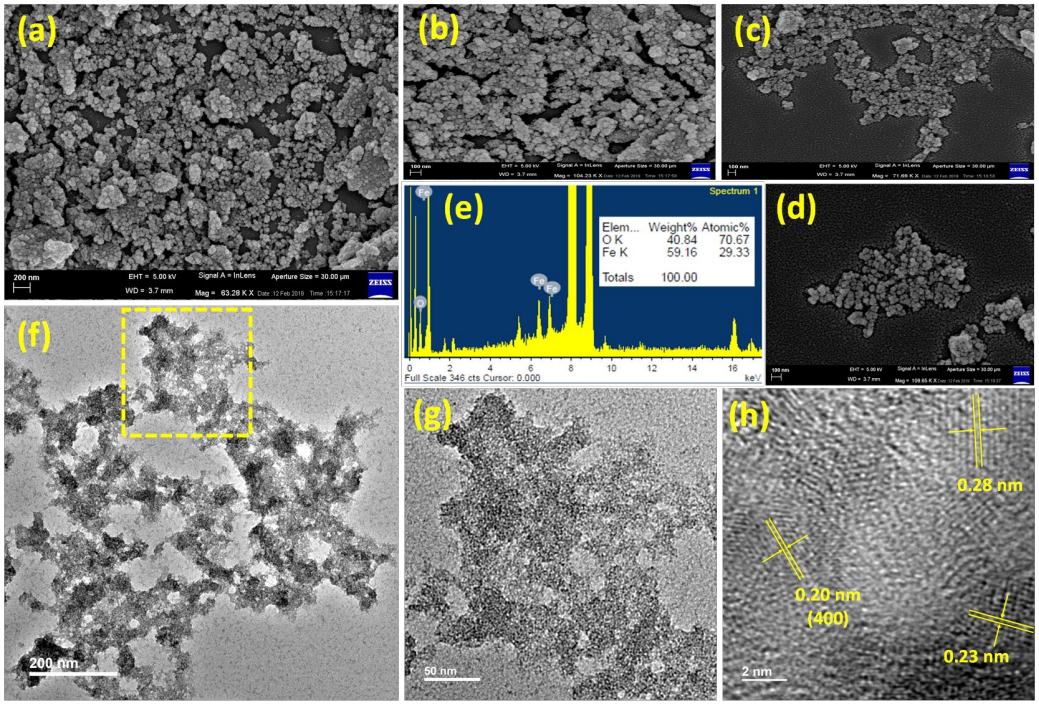

Figure S8. (a-d) FESEM images, (e) EDS data, (f, g) TEM images and (h) HRTEM image of $Fe(OH)_3$ electrocatalyst.

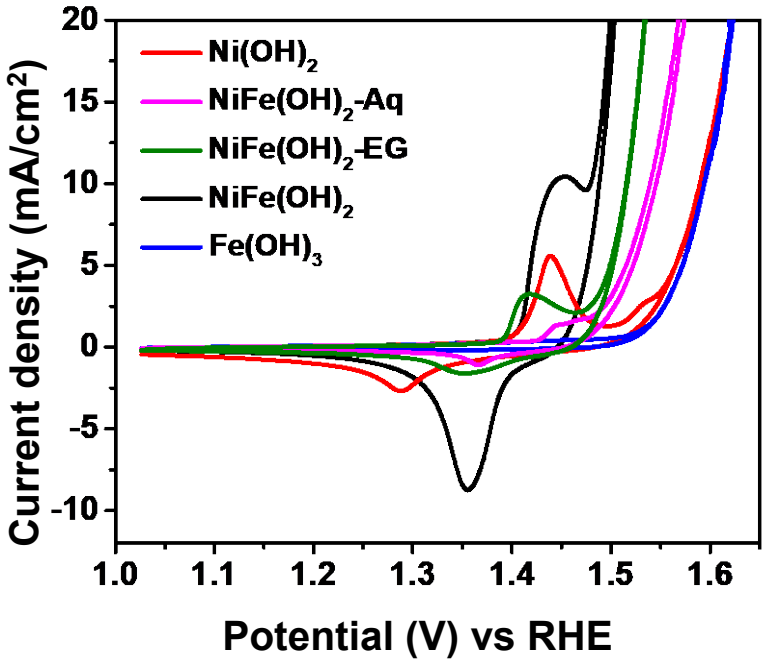

Figure S9. Polarization CV curves (iR-corrected) of $Ni(OH)_2$, $NiFe(OH)_2$-Aq, $NiFe(OH)_2$-EG, $NiFe(OH)_2$ and $Fe(OH)_3$ electrocatalysts.

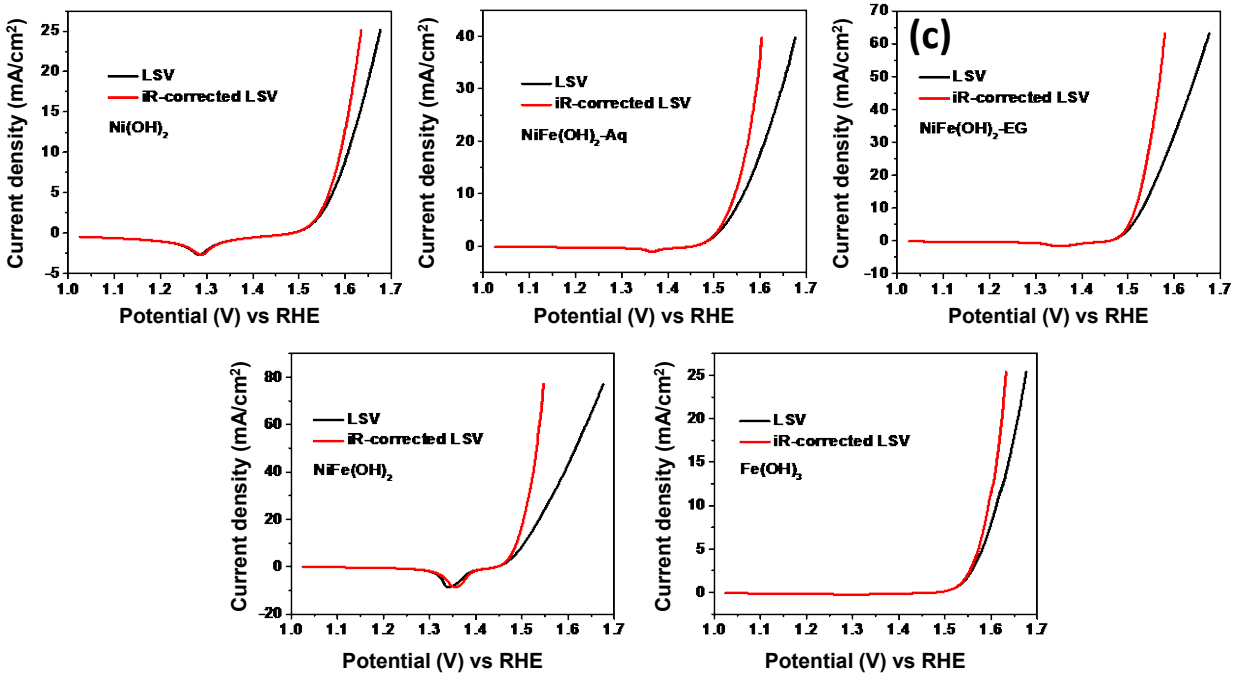

Figure S10. Backward LSV curves with and without iR-correction: (a) $Ni(OH)_2$, (b) $NiFe(OH)_2$-Aq, (c) $NiFe(OH)_2$-EG, (d) $NiFe(OH)_2$ and (e) $Fe(OH)_3$ electrocatalysts.

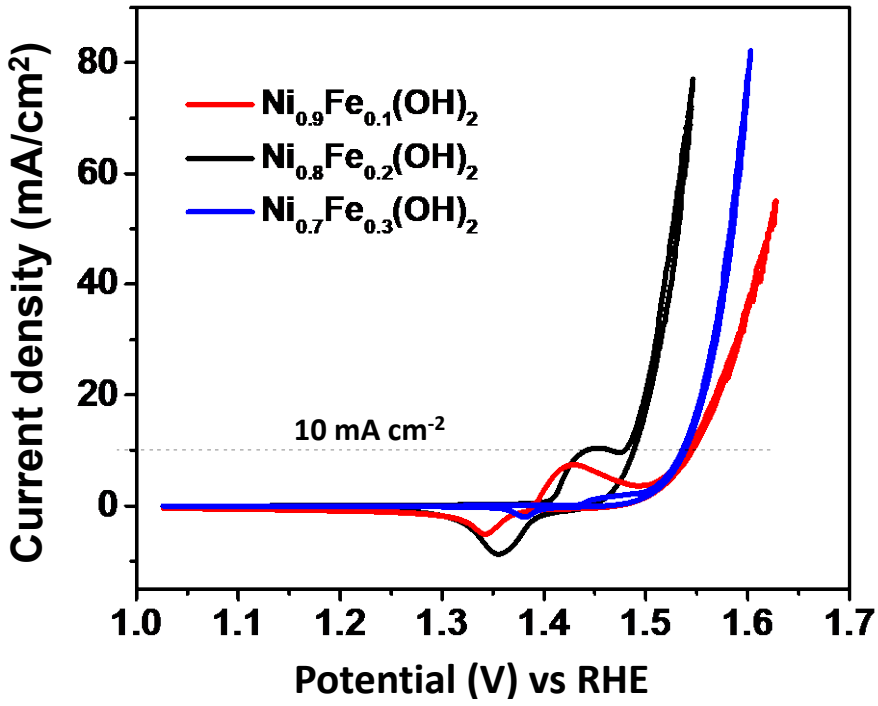

Figure S11. Polarization CV curves (iR-corrected) of $NiFe(OH)_2$ by varying the ratio of Ni and Fe.

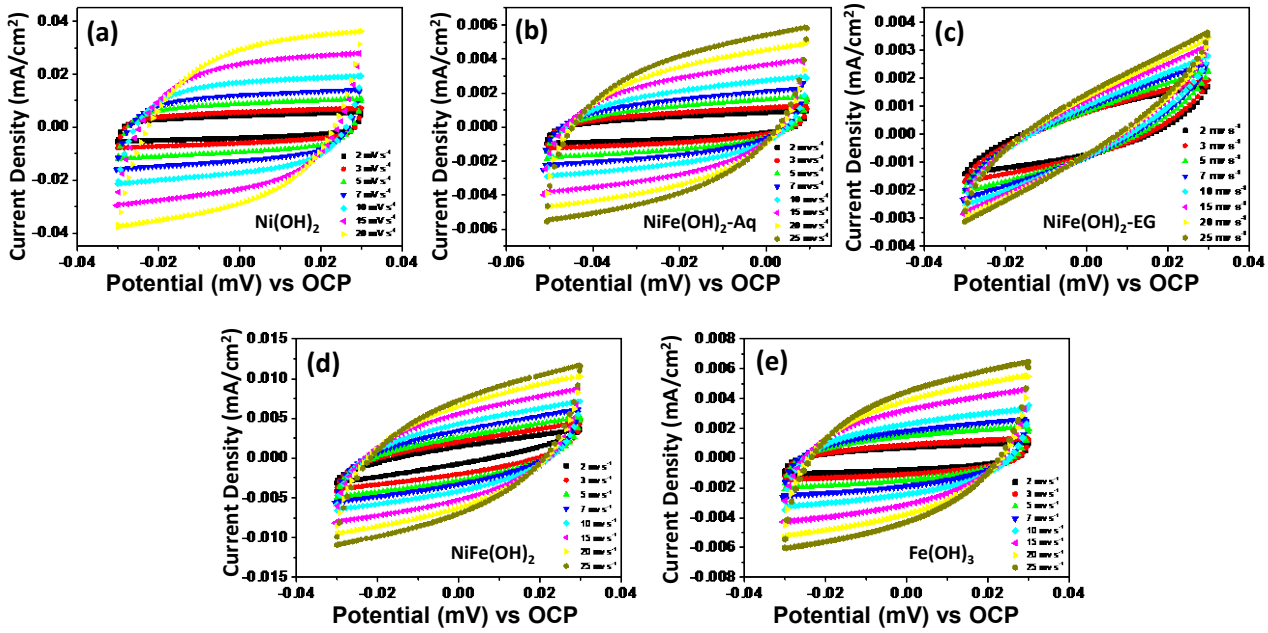

Figure S12. C_{dl} curves with different scan rate: (a) $Ni(OH)_2$, (b) $NiFe(OH)_2$-Aq, (c) $NiFe(OH)_2$-EG, (d) $NiFe(OH)_2$ and (e) $Fe(OH)_3$ electrocatalysts.

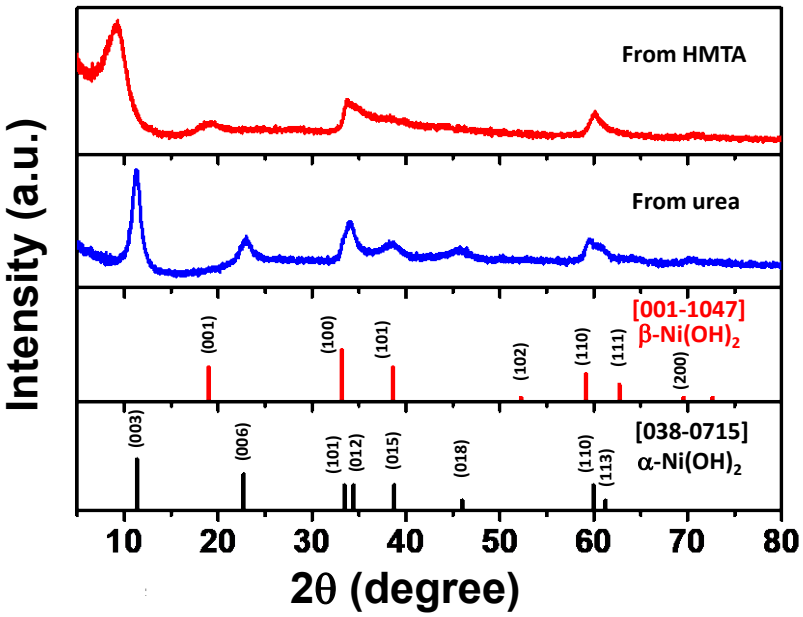

Figure S13. PXRD patterns of $NiFe(OH)_2$ prepared using bases HMTA and urea with the standard patterns of $Ni(OH)_2 \cdot 0.75H_2O$ [ICDD #038-0715] and $Ni(OH)_2$ [ICDD #001-1047].

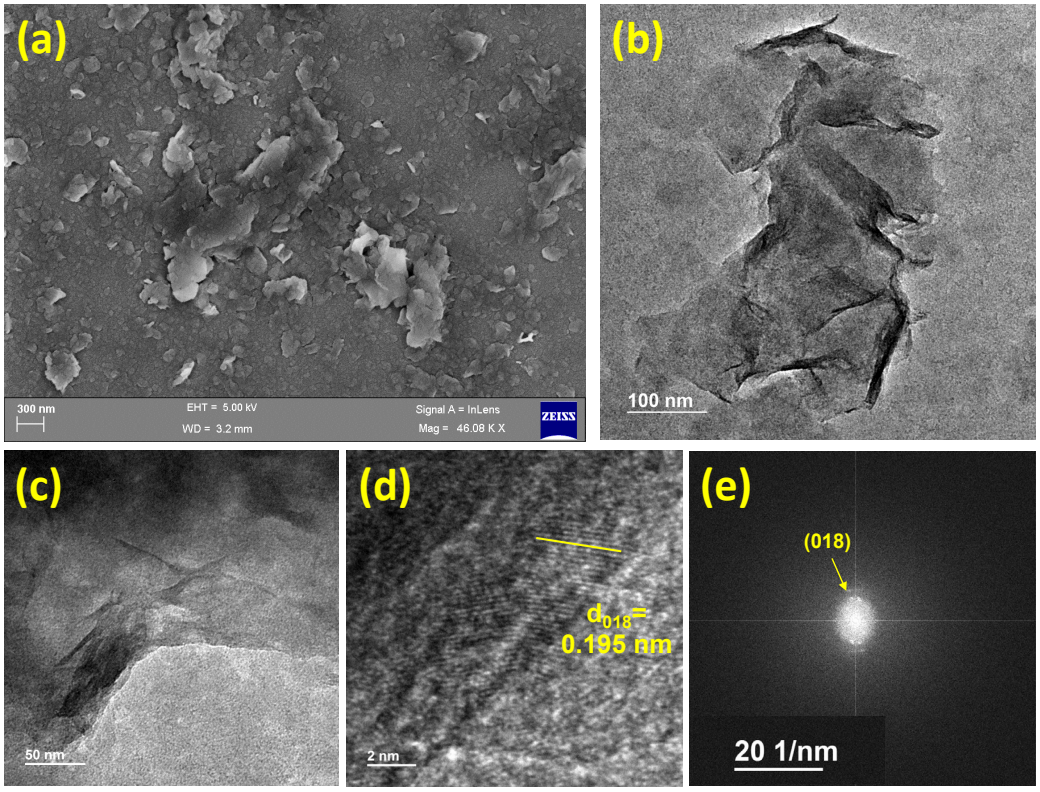

Figure S14. Morphology analysis: (a) FESEM image, (b, c) TEM images, (d, e) HRTEM image and its corresponding FFT of $NiFe(OH)_2$ prepared using HMTA.

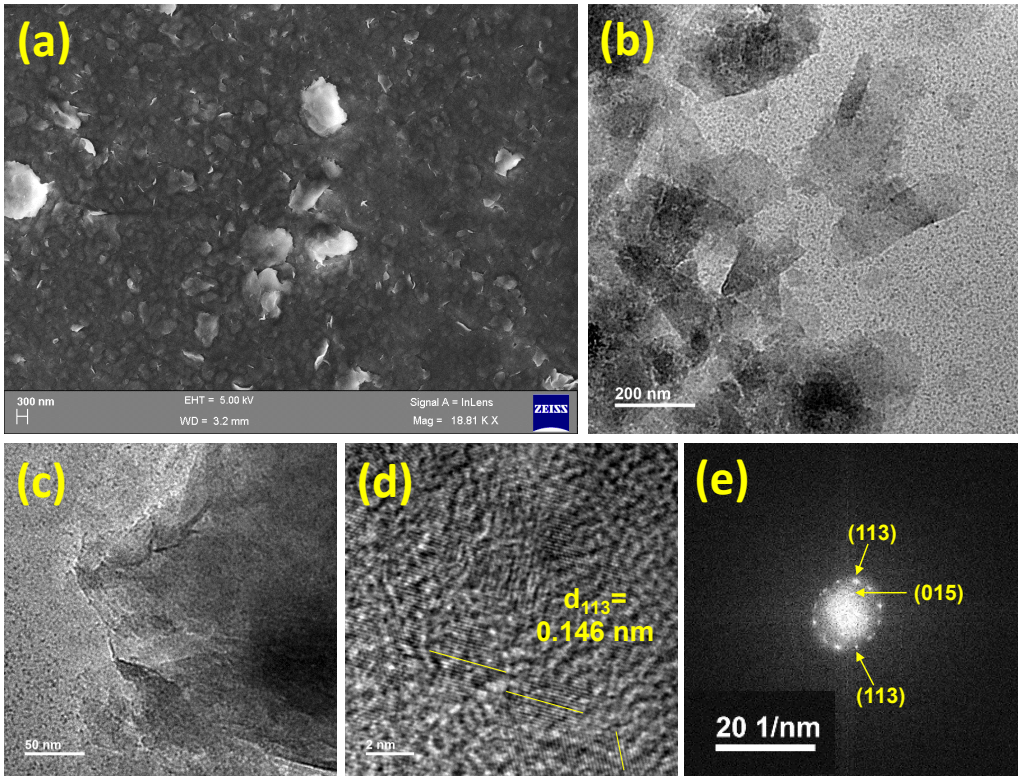

Figure R15. Morphology analysis: (a) FESEM image, (b, c) TEM images, (d, e) HRTEM image and its corresponding FFT of $NiFe(OH)_2$ prepared using urea.

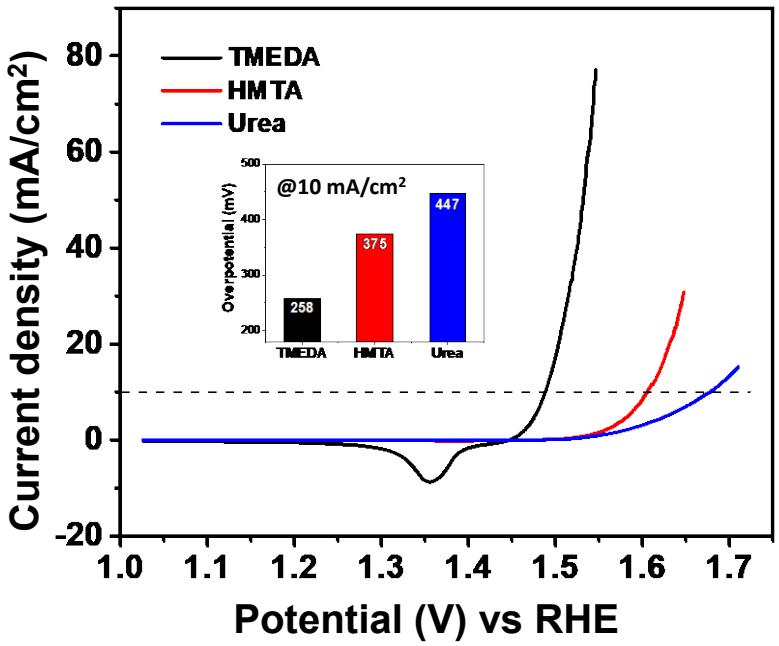

Figure S16. Polarization backward LSV curves (iR-corrected) of $NiFe(OH)_2$ prepared using different bases: TMEDA, HMTA and urea.

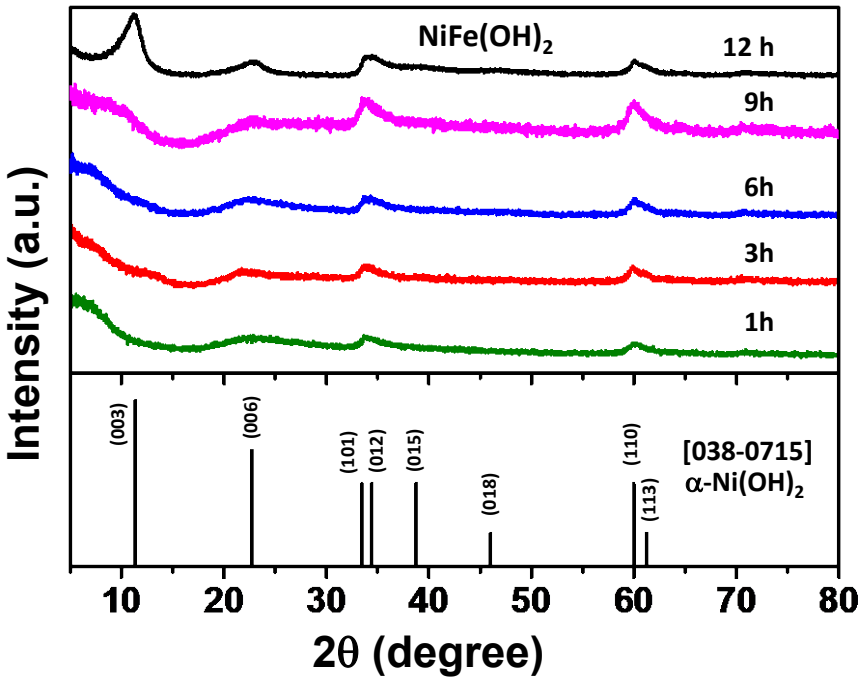

Figure S17. PXRD patterns of $NiFe(OH)_2$ prepared using TMEDA with different reaction time (1h, 3h, 6h, 9h and 12h) and the standard pattern of $Ni(OH)_2 \cdot 0.75H_2O$ [ICDD #038-0715].

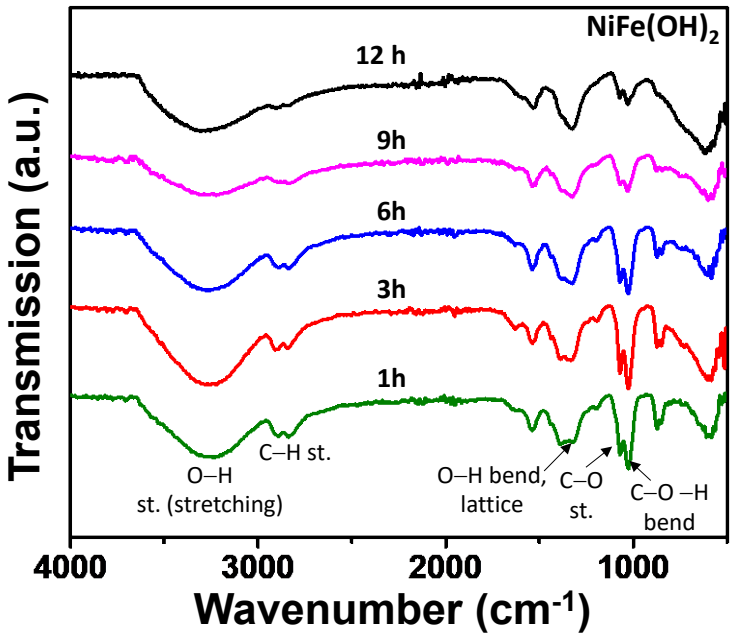

Figure S18. The FTIR spectra of $NiFe(OH)_2$ prepared using TMEDA with different reaction time (1h, 3h, 6h, 9h and 12h).

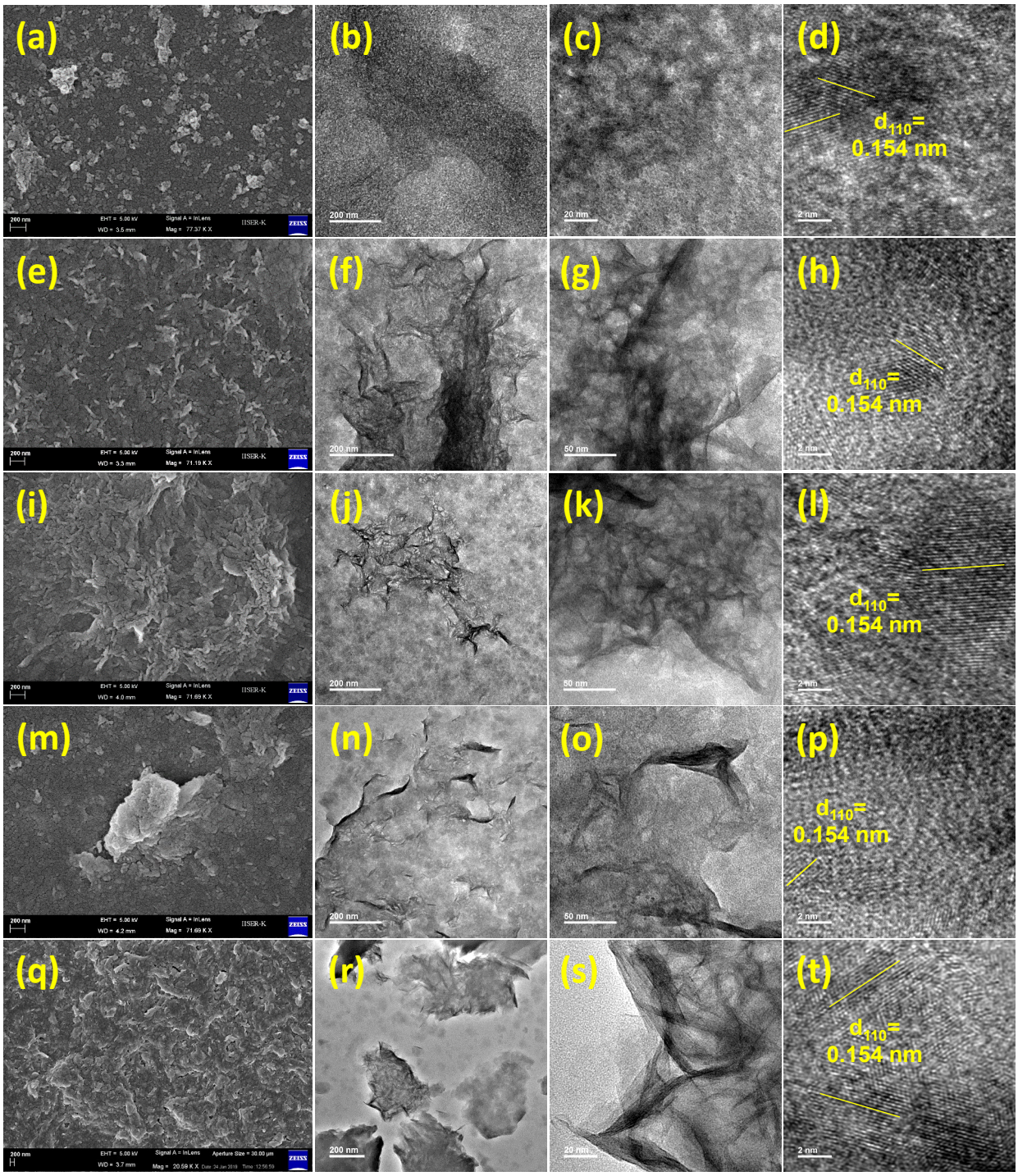

Figure S19. Morphological formation: FESEM, TEM and HRTEM images of $NiFe(OH)_2$ prepared using TMEDA with different reaction time, (a-d) for 1h, (e-h) for 3h, (i-l) for 6h, (m-p) for 9h and (q-t) for 12h.

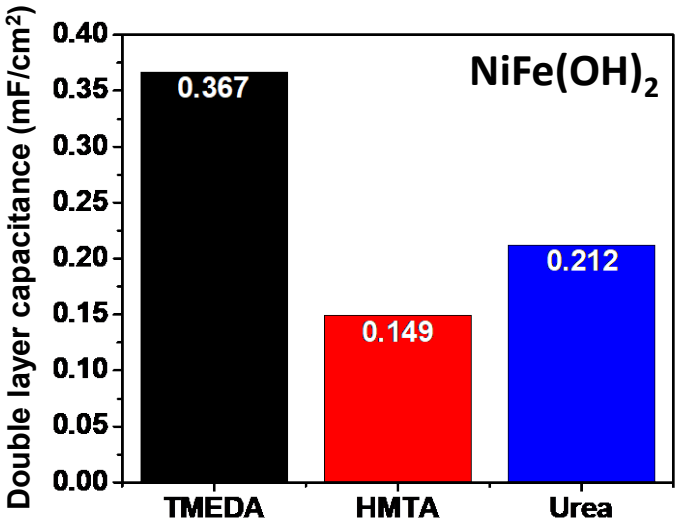

Figure S20. C_{dl} data plot for $NiFe(OH)_2$ prepared using different bases TMEDA, HMTA and urea.

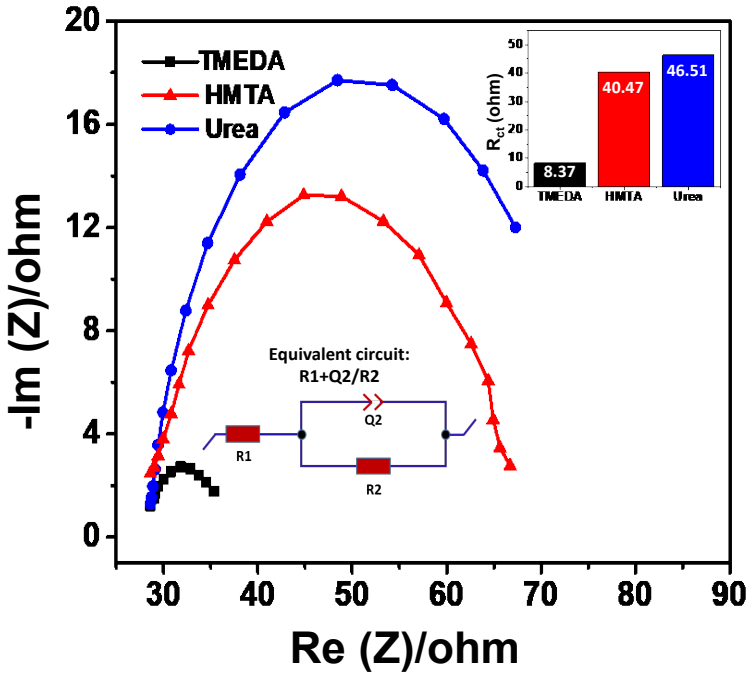

Figure S21. Nyquist plot and corresponding equivalent circuit of $NiFe(OH)_2$ materials prepared using different bases: TMEDA, HMTA and urea.

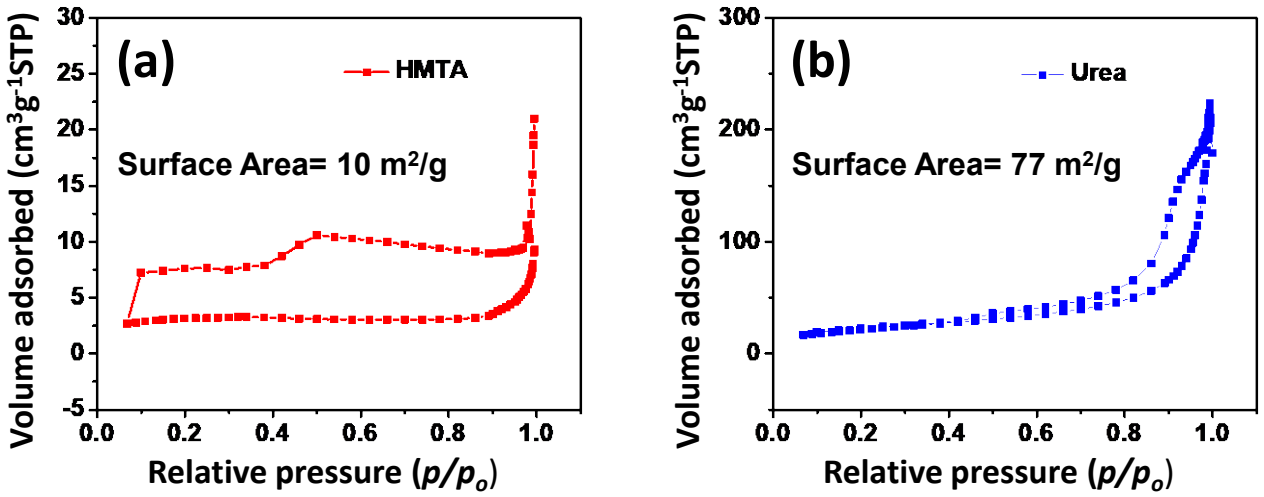

Figure S22. Nitrogen adsorption-desorption isotherms for $NiFe(OH)_2$ materials prepared using (a) HMTA and (b) urea.

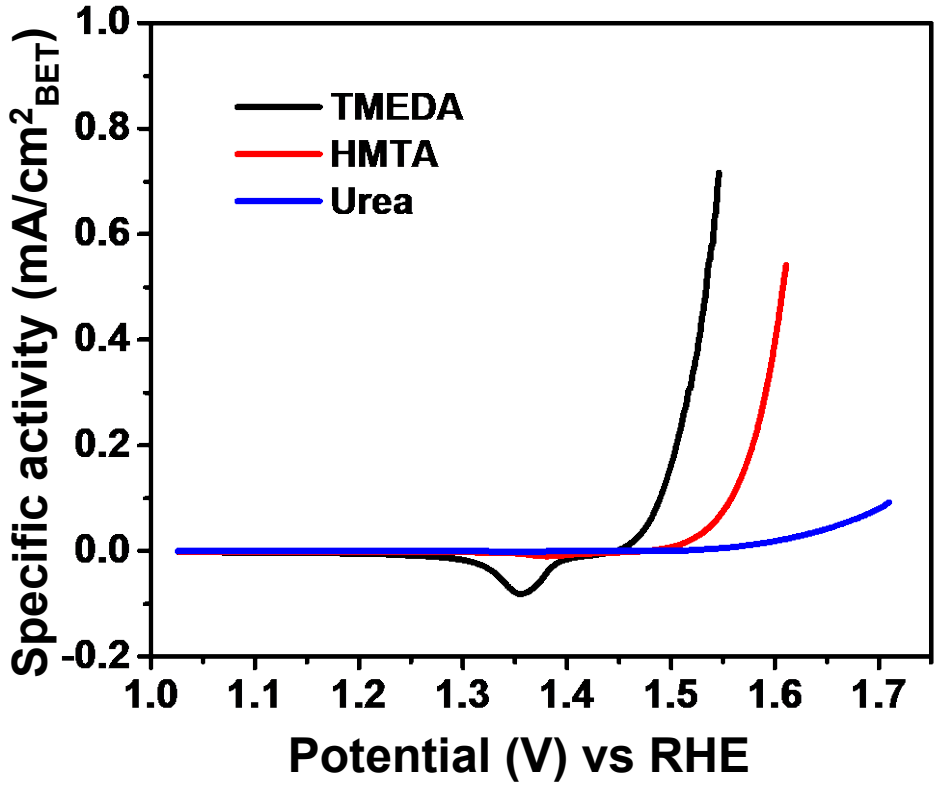

Figure S23. Backward LSV polarization curves for specific activity (BET surface area normalized) of $NiFe(OH)_2$ materials prepared using TMEDA, HMTA and urea.

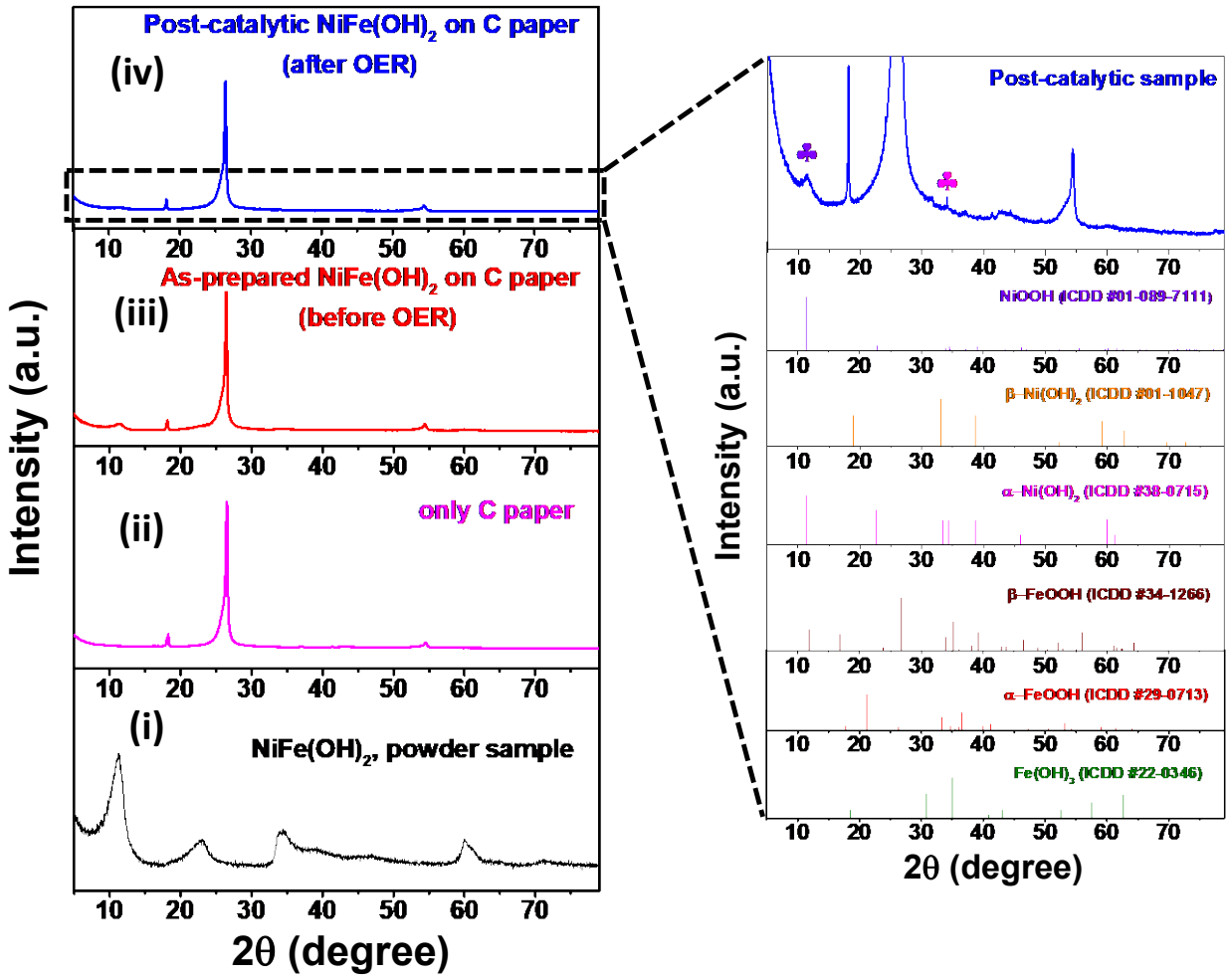

Figure S24. PXRD patterns of (i) $NiFe(OH)_2$ powder sample, (ii) only C paper, (iii) as-prepared $NiFe(OH)_2$ on C paper and (iv) post-catalytic sample on C paper, which is magnified and compared with standard patterns of NiOOH, β-$Ni(OH)_2$, α-$Ni(OH)_2$, β-FeOOH, α-FeOOH and $Fe(OH)_3$ for post-catalytic analysis.

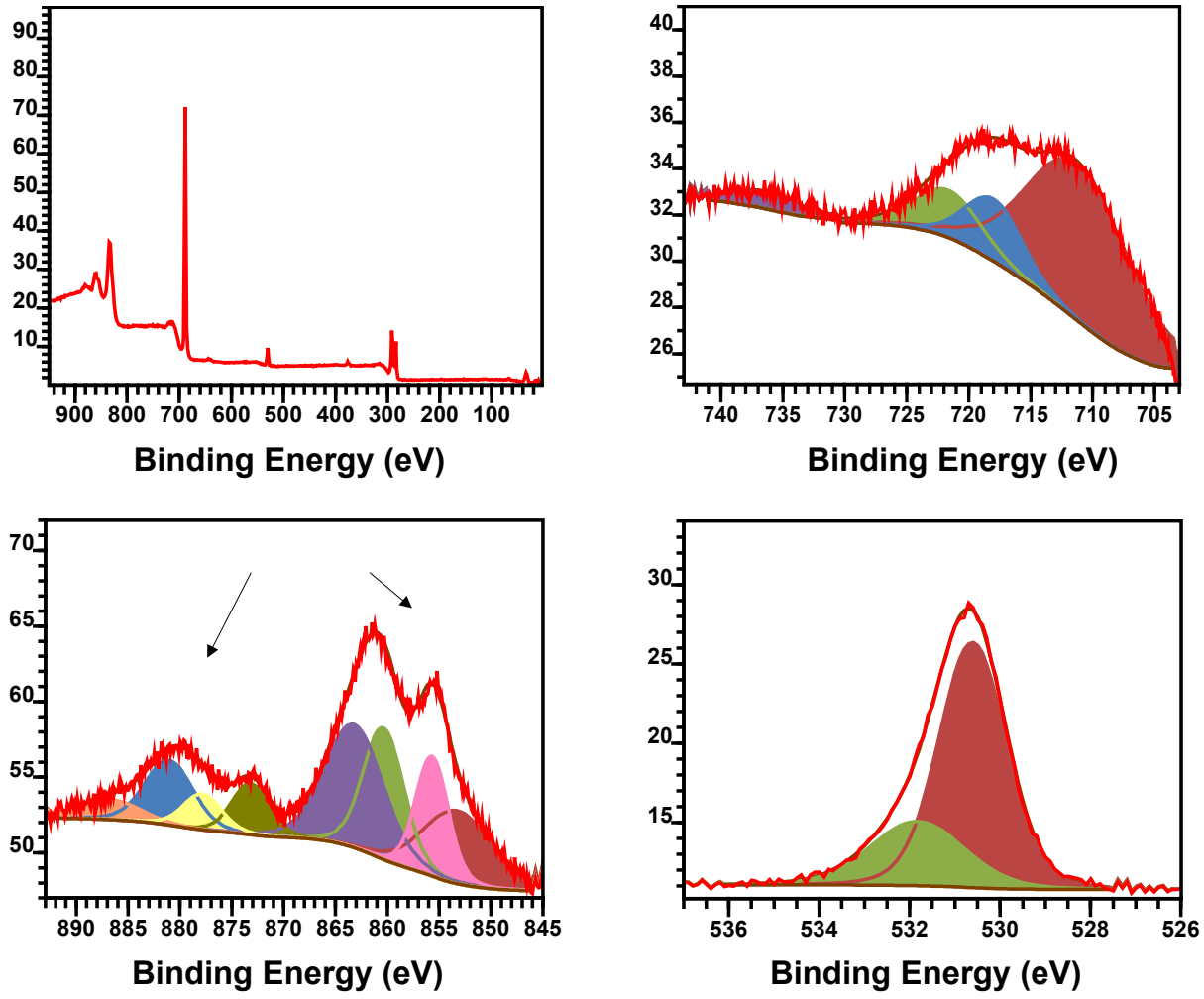

Figure S25. XPS spectra of post-catalytic sample: (a) Survey scan, (b) Fe 2p, (c) Ni 2p and (d) O 1s.

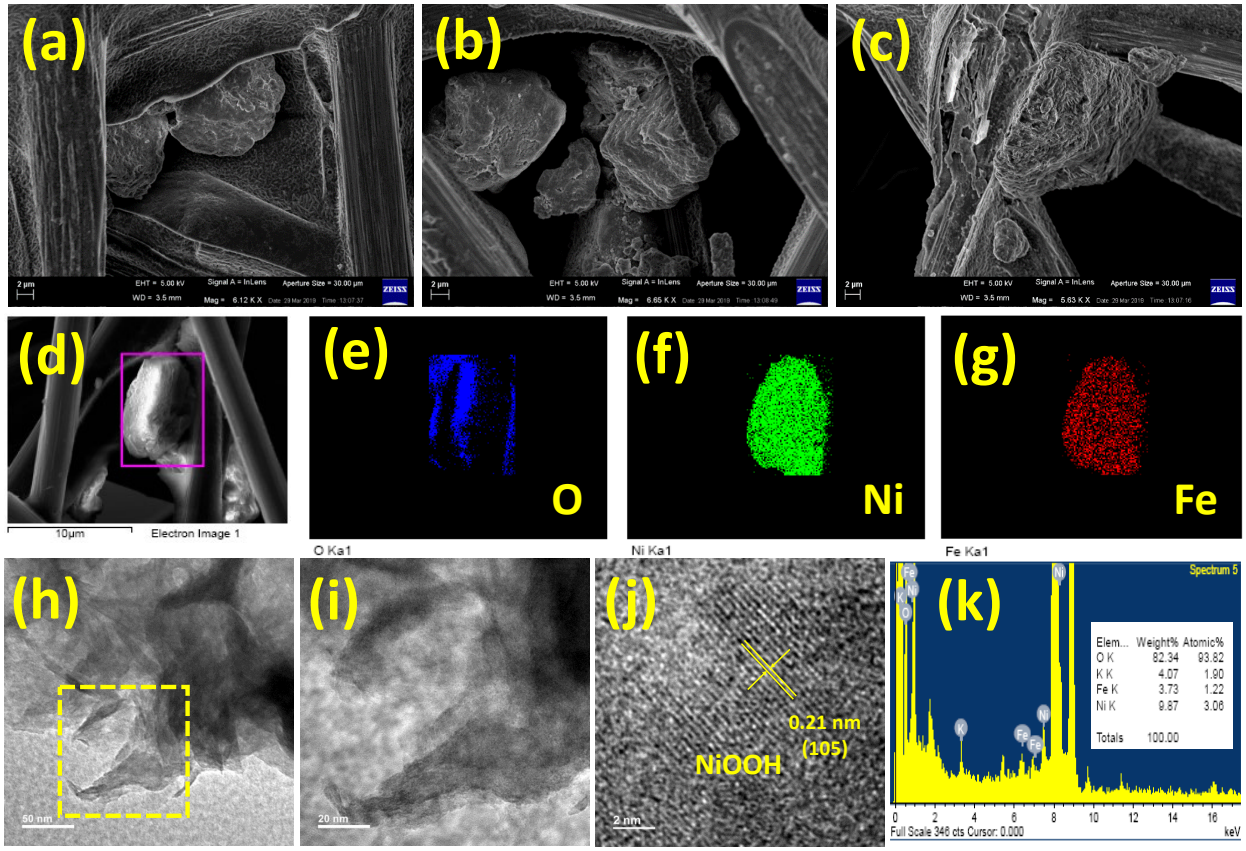

Figure S26. Morphology analysis of post-catalytic sample: (a-c) FESEM images (on C paper), (d-g) elemental mapping, (h, i) TEM images, (j) HRTEM image and (k) EDS data of post-catalytic sample.

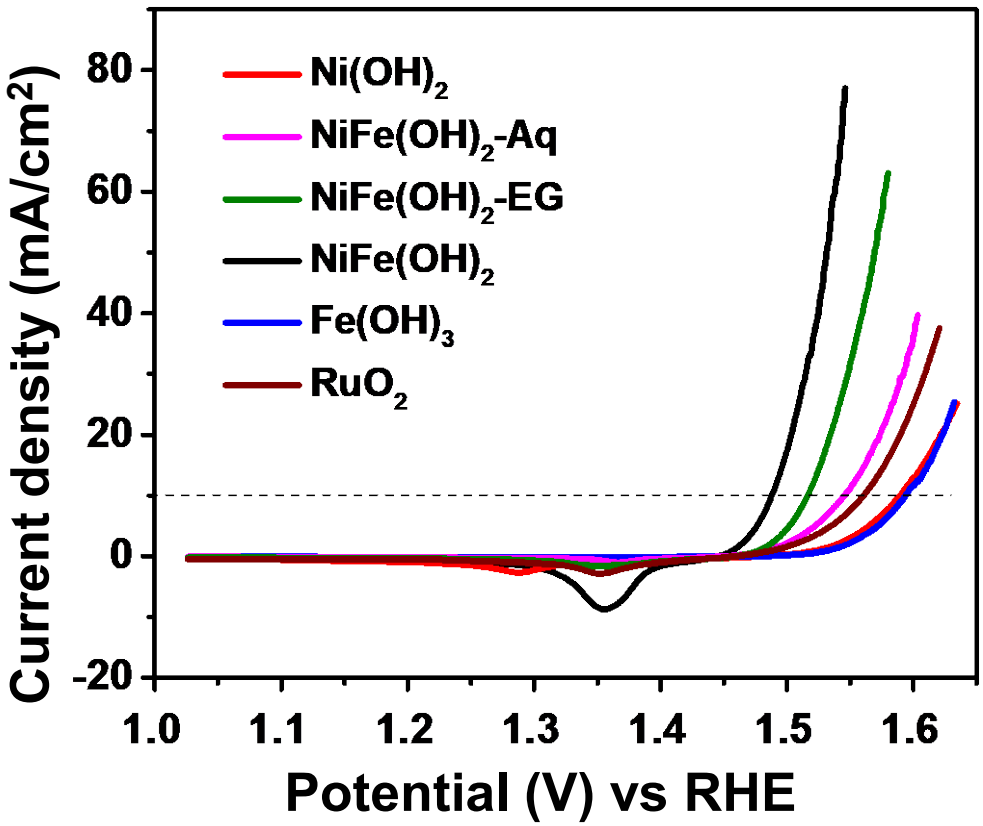

Figure S27. Comparison of backward LSV curves (iR-corrected) of $Ni(OH)_2$, $NiFe(OH)_2$-Aq, $NiFe(OH)_2$-EG, $NiFe(OH)_2$, and $Fe(OH)_3$ with RuO_2 electrocatalyst.

Tables:

Table S1: The abbreviations of as-prepared samples with the precursors used in the synthesis

S/N	Sample Details	Sample ID
1	$Ni(OCOCH_3)_2 \cdot 4H_2O + H_2O + EG + TMEDA$	$Ni(OH)_2$
2	$Fe(NO_3)_3 \cdot 9H_2O + H_2O + EG + TMEDA$	$Fe(OH)_3$
3	$Ni(OCOCH_3)_2 \cdot 4H_2O + Fe(NO_3)_3 \cdot 9H_2O + H_2O + EG + TMEDA$	$NiFe(OH)_2$
4	$Ni(OCOCH_3)_2 \cdot 4H_2O + Fe(NO_3)_3 \cdot 9H_2O + H_2O + TMEDA$	$NiFe(OH)_2$-Aq
5	$Ni(OCOCH_3)_2 \cdot 4H_2O + Fe(NO_3)_3 \cdot 9H_2O + EG + TMEDA$	$NiFe(OH)_2$-EG

Table S2. Inductively coupled plasma atomic emission spectroscopy (ICP-AES) data

Sample	Ni (ppm)	Fe (ppm)	Molar ratio of Ni: Fe
$NiFe(OH)_2$ as-prepared	18.706	4.206	4.23: 1
$NiFe(OH)_2$ post-catalysis	0.171	0.05	3.25: 1

Table S3. Surface area and porosity features of different materials as obtained from nitrogen adsorption-desorption measurement

Sample ID	BET surface area (m^2/g)	Pore Volume (cm^3/g)	Pore Size (nm)
$Ni(OH)_2$	64	0.0189	5.6
$NiFe(OH)_2$-Aq	52	0.1472	6.4
$NiFe(OH)_2$-EG	126	0.1438	3.9
$NiFe(OH)_2$	50	0.0135	3.5
$Fe(OH)_3$	267	0.2116	3.6

Table S4. Summary of the obtained values of electrochemical parameters for different electrocatalysts

Sample ID	Overpotential (mV)	Tafel slope (mV/dec)	R_{ct} (Ohm)
$NiFe(OH)_2$	258	43	8.37
$NiFe(OH)_2$-EG	286	47	15.72
$NiFe(OH)_2$-Aq	316	63	26.46
$Ni(OH)_2$	359	65	44.88
$Fe(OH)_3$	364	67	48.63

Table S5. Comparison of some of the recently reported Ni/Fe-based electrocatalysts toward OER under alkaline condition

S/N	Catalyst	Working electrode	Overpotential (mV)	Tafel slope (mV/decade)	Stability Study (h)	Conditions: Loading (mg/cm^2), electrolyte	Reference
1	**$Ni_{0.8}Fe_{0.2}(OH)_2$**	**GC**	**η_{10}=258**	**43**	**168**	**0.215, 1 (M) KOH**	**This work**
2	Fe: $Ni(OH)_2$ MP/CC 1:3	Modified CC	η_{100}=270	40	20	NA, 1 (M) KOH	*Chem. Commun.*, **2019**, 55, 10138-10141.
3	$Ni_{0.78}Fe_{0.22}(OH)_2$	Rotating disk GC	η_{10}=315	35	48	0.07, 1 (M) KOH	*ACS Appl. Energy Mater.*, **2019**, 2, 1961-1968.
4	Ni_{65}+$Fe_{35}(O_xH_y)$	GC	η_{10}=298	37	NA	~0.1, 0.1 (M) KOH	*Chem. Commun.*, **2019**, 55, 818.
5	$Ni_{2.85}Fe_{0.15}(NO_3)_2(OH)_4$	GC	η_{10}=349	121	0.83	NA 1 (M) KOH	*Int. J. Hydrog. Energy*, **2019**, 44, 10627-10636.
6	$Fe_{0.06}Ni_{0.94}(OH)_2$/ NiOOH on CC	CC	η_{10}=200	48	24	3.0 1 (M) KOH	*ChemElectroChem*, **2019**, 6, 3488-3498.

7	Fe@$Ni(OH)_2$ on Ni foam	Ni foam	η_{100} = 312	44.2	100	NA, 1 (M) KOH	*Chem. Commun*., **2018**, 54, 3262-3265.
8	Fe-doped $Ni(OH)_2$ /Ni foam	Ni foam	η_{20} =271 η_{100} =318	72	20	NA, 1 (M) KOH	*Nanoscale*, **2018**, 10, 10620-10628.
9	iron-doped nickel hydroxide on Ni foam	Ni foam	η_{100} =312	44.2	100	1 (M) KOH	Chem. Commun., **2018**, 54, 3262-3265.
10	Fe doped $Ni(OH)_2$/NiOOH nanosheets on CC	CC	η_{10} =200	48	24	3.0 1 (M) KOH	ChemElectroChem **2019**, 6, 3488–3498.
11	$Ni_{1-x}Fe_xOOH$ thin films	gold rotating disc	η_{10} =320	45	38	1 (M) KOH	J. Phys. Chem. C **2015**, 119, 18303−18316.
12	Porous Ni-Fe mixed oxides	indium tin oxide (ITO)	η_{10} =328 η_{50} =420	42	12	1 (M) KOH	Adv. Sci. **2015**, 2, 1500199.

GC= Glassy carbon, CC= Carbon cloth